REPORT DOCUMENTATION PAGE

Form Approved OMB NO. 0704-0188

1. REPORT DATE (DD-MM-YYYY)	2. REPORT TYPE	3. DATES COVERED (From - To)
06-05-2012	Final Report	1-Jun-2007 - 28-Feb-2011

4. TITLE AND SUBTITLE

NACHOS Project Final Report_University of Michigan
Optically pumped subwavelength lasers operated at room temperature

5a. CONTRACT NUMBER
W911NF-07-1-0313

5b. GRANT NUMBER

5c. PROGRAM ELEMENT NUMBER
7D10AI

6. AUTHORS

P.C. Ku, L.J. Guo, P.K. Bhattacharya

5d. PROJECT NUMBER

5e. TASK NUMBER

5f. WORK UNIT NUMBER

7. PERFORMING ORGANIZATION NAMES AND ADDRESSES

University of Michigan - Ann Arbor
Regents of the University of Michigan
3003 S. State St
Ann Arbor, MI 48109 -1274

8. PERFORMING ORGANIZATION REPORT NUMBER

9. SPONSORING/MONITORING AGENCY NAME(S) AND ADDRESS(ES)

U.S. Army Research Office
P.O. Box 12211
Research Triangle Park, NC 27709-2211

10. SPONSOR/MONITOR'S ACRONYM(S)
ARO

11. SPONSOR/MONITOR'S REPORT NUMBER(S)
53044-EL-DRP.8

12. DISTRIBUTION AVAILIBILITY STATEMENT

Approved for Public Release; Distribution Unlimited

13. SUPPLEMENTARY NOTES

The views, opinions and/or findings contained in this report are those of the author(s) and should not contrued as an official Department of the Army position, policy or decision, unless so designated by other documentation.

14. ABSTRACT

we have proposed, theoretically designed, and experimentally demonstrated three types of sub-wavelength semiconductor lasers covering different emission wavelength range. These are nanoring laser based on plasmonic confinement, Nanowire laser embedded in photonic crystals and coupled microdisk laser achieving the highest spontaneous emission coupling coefficients. Room temperature operation by optical pumping have been achieved.

15. SUBJECT TERMS

nanolaser, coherent light source, plasmonics, nanowire, microcavity

16. SECURITY CLASSIFICATION OF:			17. LIMITATION OF ABSTRACT	15. NUMBER OF PAGES	19a. NAME OF RESPONSIBLE PERSON
a. REPORT	b. ABSTRACT	c. THIS PAGE			L. Jay Guo
UU	UU	UU	UU		19b. TELEPHONE NUMBER: 734-647-7718

Report Title

NACHOS Project Final Report_University of Michigan
Optically pumped subwavelength lasers operated at room temperature

ABSTRACT

we have proposed, theoretically designed, and experimentally demonstrated three types of sub-wavelength semiconductor lasers covering different emission wavelength range. These are nanoring laser based on plasmonic confinement, Nanowire laser embedded in photonic crystals and coupled microdisk laser achieving the highest spontaneous emission coupling coefficients. Room temperature operation by optical pumping have been achieved.

Enter List of papers submitted or published that acknowledge ARO support from the start of the project to the date of this printing. List the papers, including journal references, in the following categories:

(a) Papers published in peer-reviewed journals (N/A for none)

Received Paper

TOTAL:

Number of Papers published in peer-reviewed journals:

(b) Papers published in non-peer-reviewed journals (N/A for none)

Received Paper

TOTAL:

Number of Papers published in non peer-reviewed journals:

(c) Presentations

Yi-Kuei Wu, Xin Tu, Yi-Hao Chen, and L. Jay Guo, "One Dimensional Photonic Crystal Microdisk Laser," IEEE Photonics Conference, Arlington, VA, 2001.

Number of Presentations: 1.00

Non Peer-Reviewed Conference Proceeding publications (other than abstracts):

Received Paper

TOTAL:

Number of Non Peer-Reviewed Conference Proceeding publications (other than abstracts):

Peer-Reviewed Conference Proceeding publications (other than abstracts):

Received Paper

TOTAL:

Number of Peer-Reviewed Conference Proceeding publications (other than abstracts):

(d) Manuscripts

Received	Paper

TOTAL:

Number of Manuscripts:

Books

Received	Paper

TOTAL:

Patents Submitted

Patents Awarded

Awards

Graduate Students

NAME	PERCENT_SUPPORTED	Discipline
Min Kim	1.00	
Yihao Chen	0.50	
Junseok Heo	1.00	
YiKuei Wu	0.50	
FTE Equivalent:	**3.00**	
Total Number:	**4**	

Names of Post Doctorates

NAME	PERCENT_SUPPORTED
FTE Equivalent:	
Total Number:	

Names of Faculty Supported

NAME	PERCENT_SUPPORTED	National Academy Member
P.C. Ku	0.15	
P.K. Bhattacharya	0.05	Yes
L. J. Guo	0.10	
FTE Equivalent:	**0.30**	
Total Number:	**3**	

Names of Under Graduate students supported

NAME	PERCENT SUPPORTED
FTE Equivalent:	
Total Number:	

Student Metrics

This section only applies to graduating undergraduates supported by this agreement in this reporting period

The number of undergraduates funded by this agreement who graduated during this period:	0.00
The number of undergraduates funded by this agreement who graduated during this period with a degree in science, mathematics, engineering, or technology fields:	0.00
The number of undergraduates funded by your agreement who graduated during this period and will continue to pursue a graduate or Ph.D. degree in science, mathematics, engineering, or technology fields:	0.00
Number of graduating undergraduates who achieved a 3.5 GPA to 4.0 (4.0 max scale):	0.00
Number of graduating undergraduates funded by a DoD funded Center of Excellence grant for Education, Research and Engineering:	0.00
The number of undergraduates funded by your agreement who graduated during this period and intend to work for the Department of Defense	0.00
The number of undergraduates funded by your agreement who graduated during this period and will receive scholarships or fellowships for further studies in science, mathematics, engineering or technology fields:	0.00

Names of Personnel receiving masters degrees

NAME
Total Number:

Names of personnel receiving PHDs

NAME
Min Kim
Yihao Chen
Junseok Heo
Total Number: 3

Names of other research staff

NAME	PERCENT SUPPORTED
FTE Equivalent:	
Total Number:	

Sub Contractors (DD882)

Inventions (DD882)

Scientific Progress

Detailed report can be found in the attachment of this report.

Technology Transfer

Subwavelength Semiconductor Lasers exploring different confinement schemes

L.J. Guo, P.C. Ku, P.K. Bhattacharya, University of Michigan, Ann Arbor, MI 48109

Problems to be addressed:

As the demand for interconnect speed and architectural complexity increases, the optical interconnect is a potential candidate for future intra- and inter-chip communications, offering a higher bandwidth at lower energy consumption. A dense optical interconnect network requires nanoscale components to be compatible with electronic components. In addition to nanoscale optical modulators, waveguides, and photodetectors, nanoscale resonators can provide most of the remaining functions that are needed including both passive signal processing such as add-drop filtering,[1] dispersion compensation,[2] and signal buffering[3] as well as active light generation and manipulation such as lasers[4] and switches. Furthermore, a ring resonator, a photonic crystal resonator, or coupled microdisk resonator can all be lithographically defined and evanescently coupled to an optical waveguide. Therefore high density integration of various resonators of wavelength dimension and different functions is possible.

1. Semiconductor Nanoring Lasers

In this DARPA project, P.C. Ku group have proposed, theoretically designed, and experimentally demonstrated a sub-wavelength ring laser with a tunable emission wavelength. The semiconductor nanoring laser is suitable for the optical interconnect application because it possesses unique advantages that include a traveling-wave cavity without a need for additional feedback structures, convenient in-plane coupling to an output waveguide, and independent control of emission wavelength from the device size.

One problem with typical nanolasers is that, due to nanolasers' innate nature of short cavity length, their free spectral range is usually very large. Therefore, it is difficult to fine-tune lasing wavelengths while scaling the laser dimensions. To mitigate this problem, metal-clad semiconductor nanoring lasers were proposed previously. The metal-cladding enables tighter confinement of electric field inside the semiconductor via a hybrid dielectric-plasmonic confinement. The nanoring laser has two parameters that control the resonance wavelength, ring diameter and width, which make it easier to control lasing wavelength and dimensions independently. For example, semiconductor nanoring laser's outer diameter can stay constant while controlling the lasing wavelength using ring width. The two parameters can be used together to optimize the cavity Q factor. This results in constant overall laser dimensions with multiple possible lasing wavelengths within a small range, making the semiconductor nanoring lasers attractive for on-chip use for a couple of reasons. Firstly, constant physical dimensions make the placement of nanoring lasers exhibiting different output wavelengths in an ultradense layout easier. Secondly, the possibility of multiple wavelengths within a small range makes on-chip wavelength-division multiplexing (WDM) possible, enabling a more efficient on-chip optical interconnect network. While it is true that gratings have been a preferred choice for

[1] B.E. Little, S.T. Chu, H.A. Haus, J.S. Foresi and J.-P. Laine, Journal of Lightwave Technology 15, 998-1005 (1997).
[2] G. Lenz and C. K. Madsen, Journal of Lightwave Technology, 17 (1999) 1248.
[3] F. N. Xia, L. Sekaric, and Y. Vlasov, Nature Photonics, 1 (2007) 65.
[4] D. R. Scifres, R. D. Burnham, and W. Streifer, Appl. Phys. Lett., 28 (1976) 681; N. Matsumoto and K. Kumabe, Jpn. J. Appl. Phys., 16 (1977) 1395

resonance wavelength control for larger laser cavities, it is quite difficult to integrate other wavelength-controlling feedback structures such as gratings into a nanoscale laser cavity because of the size. Therefore, as dimensions become smaller, multiple design parameters give an added advantage of wavelength control. In this project, we experimentally demonstrated a metal-clad sub-wavelength nanoring laser with a 1.2-μm diameter ($0.9\lambda_o$) and $0.8\lambda_o$ height using plasmonic structures. Furthermore, we demonstrated the tuning of the lasing wavelength via the ring width while keeping the laser dimensions constant.

Scanning electron micrographs of a semiconductor nanoring laser of 1.2-μm diameter before and after the metal deposition are shown in Fig. 1. The device diameter is defined as the outer diameter of the semiconductor part of the ring. According to 3D FDTD simulation, it is a single-transverse-mode laser. Micro-photoluminescence (μ-PL) measurement was carried out to demonstrate lasing in the 1.2-μm metal-clad nanoring cavity. The measurement was performed with the substrate kept at 10K to minimize non-radiative recombination processes. A standard μ-PL was used with a 1064 nm wavelength continuous-wave (CW) pump laser. Spontaneous emission was collected by an objective lens with a numerical aperture of 0.55, which was subsequently dispersed by a 0.5-m focal-length monochrometer and detected by a cooled InGaAs photodetector. Results of the measurement are shown in Fig. 2. Progression of a lasing peak is clearly seen in the figure. Along with the stimulated emission, spontaneous emission also becomes broader. The PL data are analyzed further, and the pump power vs. peak PL intensity is plotted in Fig. 3. Transition from spontaneous to stimulated emission occurred at the pump power of 10 mW. Of the 10 mW of pump power, only a small fraction actually corresponds to pump absorbed by the active region. Assuming a 6-μm diameter of focused laser spot, the actual absorbed power is 50 μW. The mode volume of the metal-clad nanoring resonator cavity of 1.2 μm diameter is calculated to be 0.004 μm^3. The 1.2-μm nanoring laser has a spontaneous emission coupling factor, β, of 0.01. The high β factor leads to decreased threshold pump power, as observed in Fig. 3.

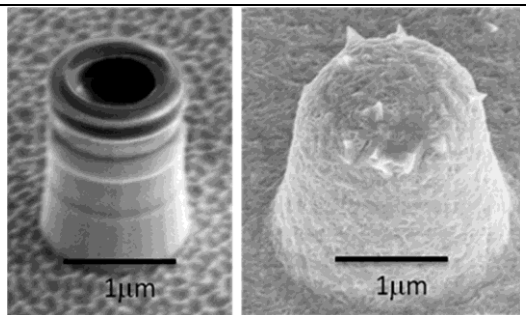

Fig. 1 SEM images of a nanoring laser after etching, prior to (left) and after (right) metal deposition.

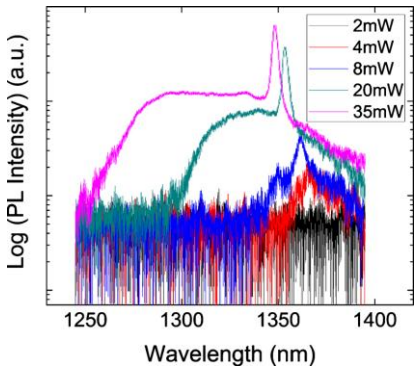

Fig. 2 Intensity-dependent μ-PL of a 1.2μm-diameter metal-clad ring laser with 250nm ring width.

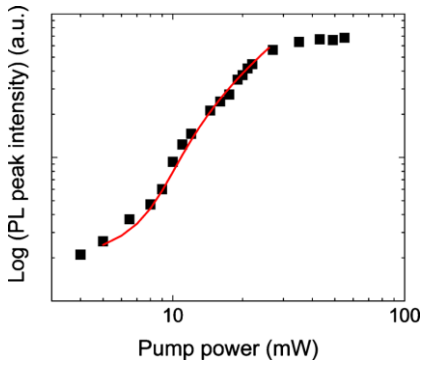

Fig. 3 Pump power vs. peak PL intensity of 1.2-μm diameter metal-clad nanoring.

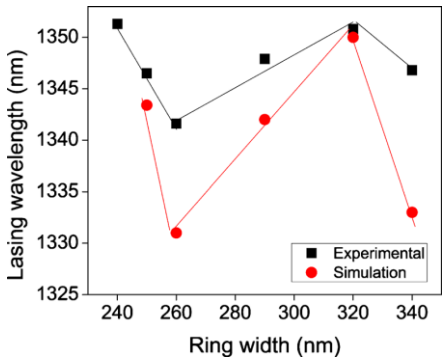

Fig. 4 Lasing wavelength shift due to ring width variation. Lines are for visual guidance only.

To demonstrate wavelength tuning, metal-clad nanoring lasers of 1.2−μm diameter with various ring widths were fabricated and measured using the identical optical measurement scheme described above. The results are shown in Fig. 4. It can be clearly seen that, by altering the ring width between 240 nm and 340 nm, the lasing wavelength can be fine-tuned to within a 10 nm range. The oscillatory behavior of the lasing wavelength is due to the shift of nearby resonance peaks in and out of the spontaneous emission range of the epi-structure. According to the 3-dimensional finite-difference-time-domain (3D-FDTD) simulations, the resonance peaks undergo a red-shift behavior with increasing ring width in general. In Fig. 4, resonance peaks within the spontaneous emission range of the epi-structure from 3D-FDTD simulations are plotted along with the experimental data. The trend agrees well with the experiment. The discrepancy of the lasing wavelengths may be due to the passive active region assumed in the calculations.

In summary, lasing in a 1.2-μm diameter sub-wavelength metal-clad nanoring resonator has been demonstrated. The emission wavelength can be tuned for a 10-nm wavelength range by changing the ring width from 240 nm and 340 nm.

2. Monolithic single GaN nanowire laser with a photonic crystal microcavity on silicon

In the last phase of this program Bhattacharya group exploited a different scheme to produce highly confined laser cavity, by embedding a semiconductor nanowire in the very center of a photonic crystal cavity. The successful catalyst-free growth of Ga(In)N nanowires of 20-100 nm diameter and lengths up to 2 μm on both (001) and (111)-oriented silicon substrates has been recently demonstrated. As shown in Figs. 5(a) and (b), the nanowire density can be varied in the range of 10^8-10^{11} cm^{-2} and the emission wavelength can be tuned, by varying the In composition, from 366 to 700 nm at room temperature. Most importantly, the nanowires grow vertically in the wurtzite crystalline form and detailed structural characterizations indicate that they are relatively defect-free (Fig. 5(c)). This is mainly due to their large surface-to-volume ratio. Consequently, there is much interest in developing nanoscale lasers using semiconductor nanowires. In this report, an optically pumped monolithic single GaN nanowire laser on silicon with a two dimensional (2D) photonic crystal (PC) resonant cavity is presented, which has a sub-wavelength modal volume, operating at room temperature.

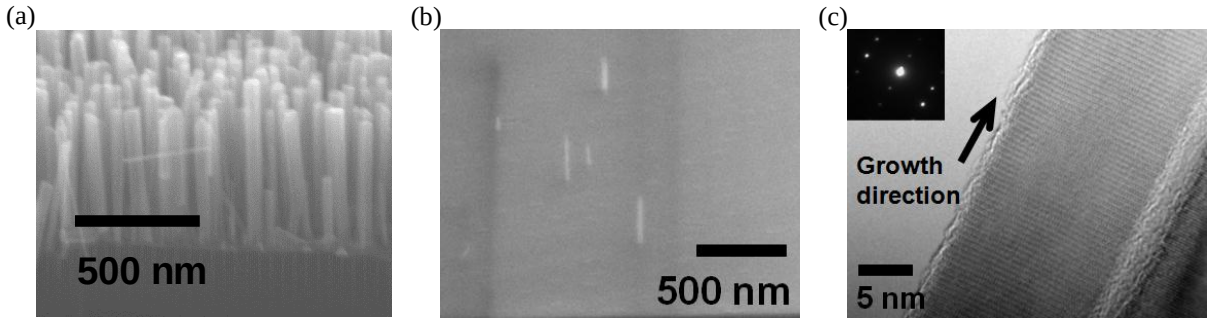

Fig. 5 (a) and (b) Cross-sectional SEM images of catalyst-free GaN nanowires grown by plasma-assisted MBE with different densities of ~1×10^{11} cm^{-2} on (001) Si (a) and ~1×10^{8} cm^{-2} on (111) Si (b); (c) high resolution TEM image of a GaN nanowire with a diameter of 20 nm which exhibits no observable defects. The inset shows the diffraction pattern indicating the nanowire is a single crystal wurtzite structure with the *c*-axis along the growth direction.

The device heterostructure, schematically shown in Fig. 6(a), consists of a single GaN nanowire at the center of a H2 defect. This single nanowire is surrounded by a 2D PC microcavity fabricated in a TiO_2 layer and a spin-on-glass (SOG) layer as a low refractive index material to reduce optical loss from the TiO_2 layer to the Si substrate. The measured optical refractive indices of SOG and TiO_2 at λ=380 nm are 1.4 and 2.5, respectively and the imaginary part of the refractive index of TiO_2 is ~0.001. As a resonator, a H2 defect PC microcavity is chosen to tolerate any alignment error in a lithography step and is designed by using the PWE method and three-dimensional (3D) finite difference time domain (FDTD) simulation.

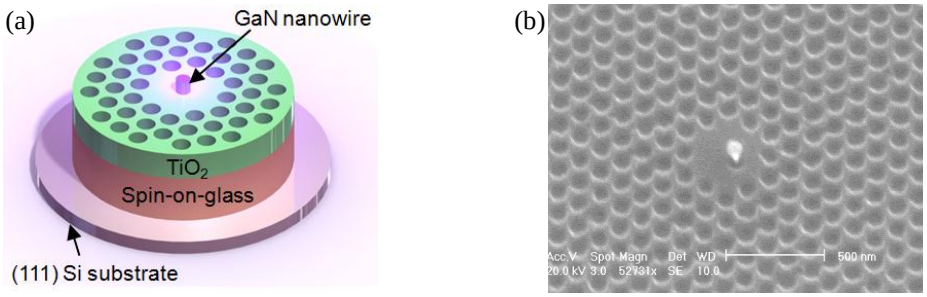

Fig. 6 (a) Schematic representation of nanowire laser consisting of a single GaN nanowire and a two dimensional photonic crystal microcavity in the TiO_2 layer (120 nm); (b) an oblique view SEM image of the fabricated device. The single GaN nanowire is well-aligned in the center of the H2 defect of the photonic crystal microcavity.

Figure 6(b) shows the fabricated device with a single nanowire aligned in the center of the H2 defect of the PC microcavity. A small hollow that is formed around the nanowire in the center of the H2 defect is due to the directional nature of TiO_2 deposition. The calculated Q-factor, mode volume, and confinement factor Γ are 570, ~0.003223 μm^3 ($0.92(\lambda/n)^3$), and 0.04, respectively. The modal gain estimated from the Q-factor is ~520 cm^{-1} and the corresponding optical gain at threshold is ~13,000 cm^{-1}, which is achievable in GaN.

The device is optically excited at room temperature with a pulsed laser at λ = 266 nm with a pulse duration of ~100 fs. Figure 3(a) shows the output spectra recorded for pump power densities of 95 kW/cm^2 (below threshold), 143 kW/cm^2 (slightly above threshold), and 477 kW/cm^2 (above threshold). At low pump power density (~95 kW/cm^2), a broad GaN bandedge

emission with a full width at half maximum (FWHM) of ~10 nm is observed. The output emission also exhibits a fairly narrow peak (~4.5 nm) at λ=370.4 nm which is believed to be due to the Purcell effect which enhances spontaneous emission. The enhanced spontaneous emission peak becomes more pronounced near threshold (120 kW/cm^2) and evolves into a coherent lasing peak above threshold. The lasing peak is made up of two transitions, indicated by the two Gaussian fitting curves, with the dominant transition having a linewidth of ~0.55 nm limited by the measurement system. To understand the origin of the dual lasing peaks, the resonant modes were calculated for different positions of the nanowire in the H2 defect. As shown in Fig. 7(b), there are two degenerate modes at a/λ = 0.2826 and 0.28267 (black lines), which are spectrally very close when the nanowire is placed in the center. As the nanowire is placed off-center in the H2 defect, the two degenerate modes becomes more separated, leading to individual modes at a/λ = 0.28167 and 0.28191 (blue lines). We therefore believe that the dual lasing peaks result from a lifting of the degeneracy of the dominant H2 cavity modes due to an off-center positioning of the GaN nanowire within the defect

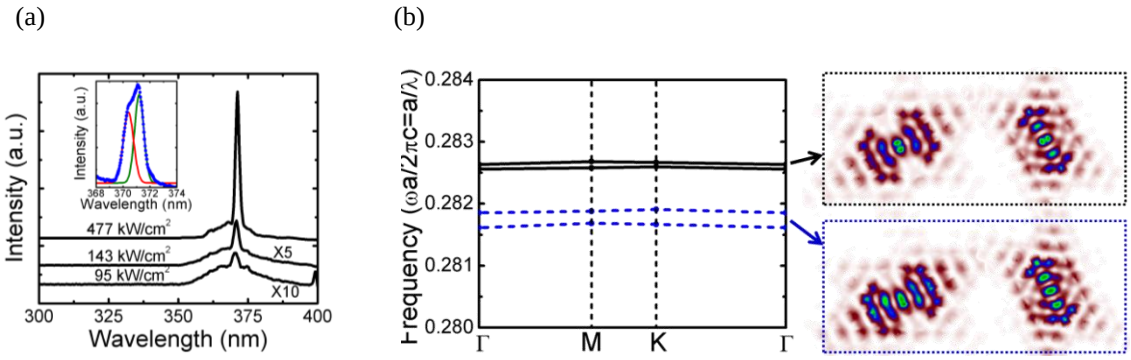

Fig. 7. (a) Photoluminescence of the laser at pump power densities of 95, 143, 477 kW/cm^2. Spectra are offset for clarity. The inset shows the lasing spectrum (blue circles), which is matched to the sum of two Gaussian peaks (green and red solid lines); (b) Calculated resonant modes with the nanowire in the center (black) and off-center by 60 nm (blue). Mode profiles of each case are shown on the right.

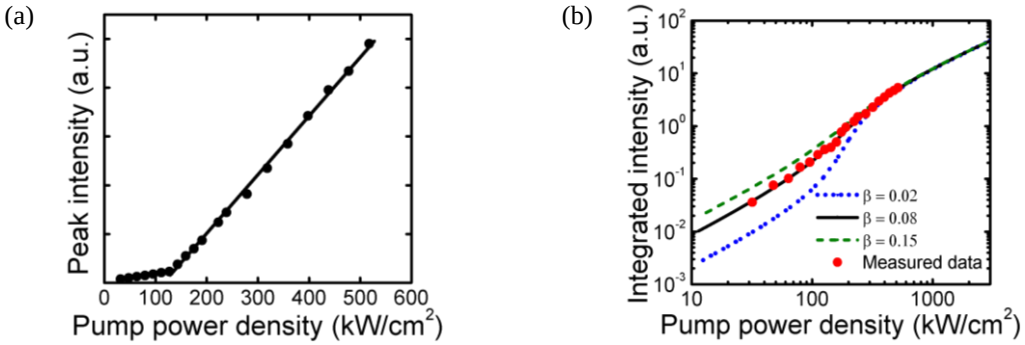

Fig. 8. (a) Variation of peak output intensity with pump power; (b) log-log plot of spectrally integrated light intensity (red circles) versus pump power density. Theoretically calculated light intensity using the rate equations is also shown for spontaneous emission factors (β) of 0.02, 0.08, and 0.15.

The measured variation of the peak intensity of the emitted light with pump power density is shown in Fig. 8(a). A clear lasing threshold is observed at a pump power density of ~120

kW/cm^2. Calculated plots of emission intensity versus pump power density on a log-log scale are shown in Fig. 8(b). Calculations were done for values of the spontaneous emission factor β of 0.02, 0.08 and 0.15. The optical gain was approximated by a linear model, $g(n)=g_0(n-n_{tr})$, where $g_0=2.5\times10^{-16}$ cm^2 and $n_{tr}=7.5\times10^{18}$ cm^{-3}. The measured integrated emission intensity versus pump power density is also plotted alongside the calculated curves. The best agreement between calculated and measured data is obtained for β = 0.08.

3. Photonic crystal microdisk lasers with exceptional spontaneous emission coupling to the lasing mode

Jay Guo group have exploited a coupled photonic molecule laser in the last year of the program. This structure is investigated as an alternative to the metal-capped microdisk laser developed earlier in the program, to address the optical loss of the surface plasmon wave. Ideally ultrahigh-efficiency semiconductor laser should have the following characteristics – high quality factor (Q), large spontaneous emission coupling factor (β), small device volume, and ease of integration. β is defined as the ratio of spontaneous emission into lasing mode to the total radiative emission; a large β will lead to reduced threshold for lasing. In this regard, different types of cavities mentioned above each has its own advantages and limitations. A long existing issue for microdisk lasers is the small spontaneous emission coupling rate (β) in microdisk. We found that it is due to the coupling of emitter spontaneous emission into competing Fabry-Perot (FP) modes in the microdisk cavity. We propose a new type of photonic crystal microdisk (PCM) laser to drastically suppress the photonic density of states in the vertical FP modes. As a result, we obtained a three-fold increase of β than previously reported highest β of 0.15 at room temperature. The spontaneous emission control in truncated photonic crystals becomes efficient when the period number is more than one. We also demonstrate a three-stack PCM laser at low temperature with β as high as 0.72, which is 24 times higher than that in typical single microdisk (0.03), which also results in 50% threshold reduction.

The primary reason for small β of WGM in microdisks is stated in the previous paragraph: strong competition between lasing and nonlasing modes. Clearly, to significantly improve β of the lasing WGM mode, suppressing radiation into all the non-desirable modes becomes crucial. This can be done by reducing $\gamma_{nonlasing}$. According to Fermi's golden rule, manipulation of the photonic density of states controls spontaneous emission. Therefore, large β to the lasing mode can be achieved by minimizing the mode density of the other competing and non-lasing modes, e.g., the FP modes in a microdisk cavity. Theoretically, the mode density can be modified effectively even by truncated 1D PhC, where the PhC structure is terminated by a bulk material with only finite pairs.

To boost β of the WGM modes in microdisk cavity, we propose a photonic crystal microdisk laser shown in Fig. 9(a). This device, consisting of multiple stacks of microdisks, is designed specifically to suppress the optical DOS in vertical direction and therefore to funnel most spontaneous emission into a lasing WGM mode. We fabricated the PCM lasers on a substrate with GaAs/AlGaAs stack structures. AlGaAs is selectively etched to make air gap as the low index layer of the PCM. A scanning electron micrograph image of the fabricated laser device is shown in Fig. 9(b). To fabricate the device, first a 300nm oxide film is deposited with plasma-enhanced chemical vapor deposition (PECVD). Then the electron beam lithography (EBL) is performed, followed by Ni deposition and a lift-off process. The resulting Nickel disk pattern is used as a hardmask in the following dry etching of the whole stack with inductively coupled

plasma reactive ion etching (ICP-RIE). The PCM structure is realized with the final step of selective etching of $Al_{0.75}Ga_{0.25}As$ in dilute buffered hydrofluoric acid.

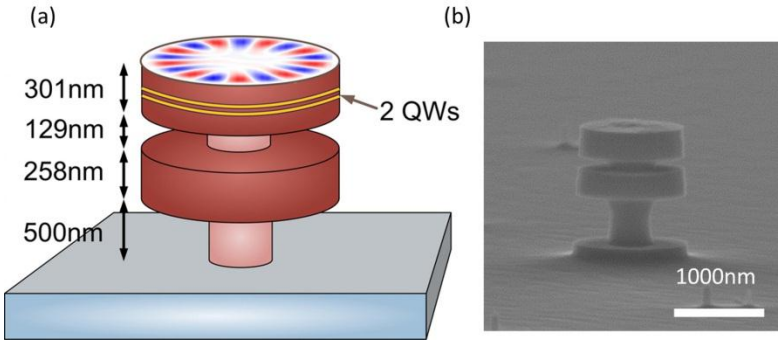

Fig. 9. (a) the schematics of the photonic crystal microdisk (PCM) laser and the field distribution of the WGM mode TE(9,1) (b) scanning electron micrograph image of PCM laser.

The measurement setup is a micro-luminescence (μ-PL) system by using a Ti:Sapphire pulsed laser as excitation source. We demonstrated a single mode PCM laser with a disk diameter of 1.2μm at room temperature. The threshold spectrum below and above threshold is presented in the logarithmic scale in the Fig. 10(a). Single mode lasing is obtained at wavelength of 969nm, in good agreement with the simulation. The 3dB bandwidth is 1.2nm, indicating an active Q of 890. Moreover, the clear cavity peak with suppressed broad spontaneous spectrum below threshold verifies that the spontaneous emission is dominated by the lasing WGM mode in the PCM structure. The colored solid curves in this graph are calculated in log-log scale for purcell factor of 5.3, whereas the threshold curve in the logarithmic scale is depicted with triangular marks in this figure. β of the two-stack PML is fitted to 0.5, which is enhanced more than 3 folds than the typical value 0.15 for a single microdisk cavity. This increasing β verifies again our hypothesis that the suppression of DOS in vertical direction helps improving the spontaneous emission coupling rate into WGM lasing mode. This experimental result matches with the simulated coupling rate.

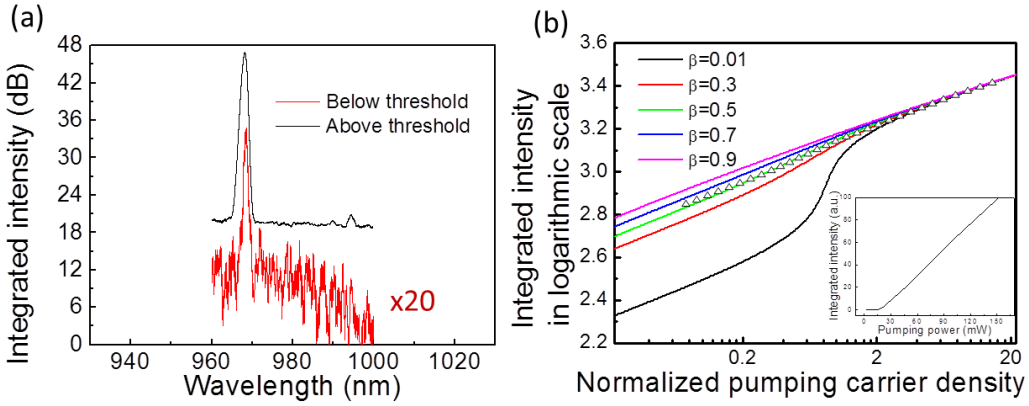

Fig. 10. (a) threshold spectrum below and above threshold of two-stack PCM in the logarithmic scale (b) The calculated threshold curve with various β(colored solid lines) and the experimental L-L curve (triangle dots). Inset illustrates the experimental L-L curve in linear scale.

To further verify that multiple pairs of photonic crystal in PCM can boost β and reduce pumping threshold, we designed a three-pair photonic crystal microdisk cavity (Fig. 11); and performed thorough coupled wave analysis. The multiple stacks result in large spontaneous emission factor ~0.72 and the inter-coupling strength ~0.39THz of optical modes between adjacent disks is at least one order of magnitude higher than the dot-cavity coupling strength (10-30GHz) that has been realized thus far. This is a distinct advantage to possibly realize the long-distance coupling between two quantum dots in different locations. We expect that vertically coupled PM microdisks will be helpful in some functional devices in QED and highly-dense photonic integrated circuits .

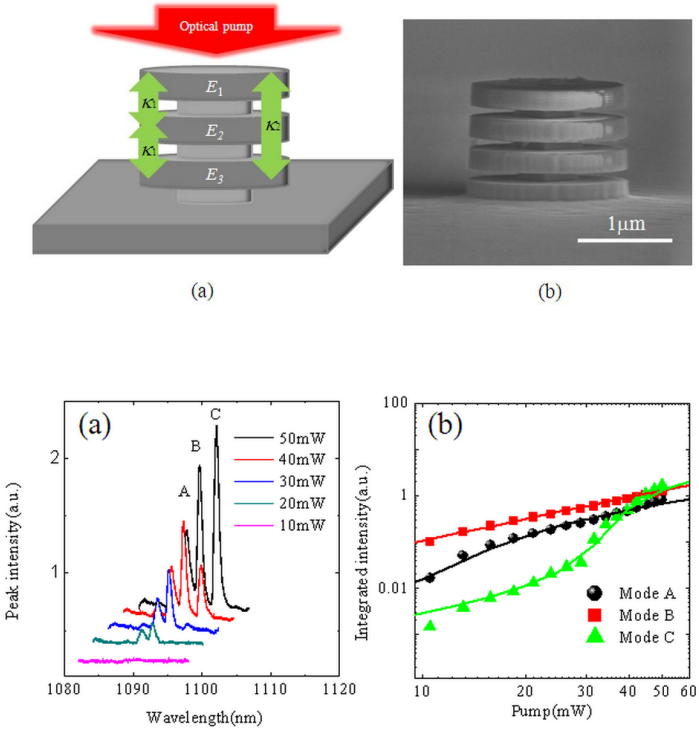

Fig. 11. (Top panel) Schematic of the PM microdisk laser and Scanning electron micrograph image of PM microlaser. Lower panel (a) Evolution of emission spectra from PM microdisk laser of 1.4□m in diameter. (b) Emission intensity vs. pump power for three supermodes. Solid lines show the rate-equation-model fit to the experimental data.

In conclusion, we have shown that photonic crystal microdisk laser cavity provides a large spontaneous emission coupling rate into whisepering gallery mode. This is achieved because the photonic density of states corresponding to the vertical FP resonances is effectively suppressed. We have also demonstrated that more than one pair of photonic crystal can give strong modification of optical density of states in the direction normal to the disk. With a greatly increased spontaneous coupling rate to the lasing WGMs with small mode volumes, this structure may pave the way for high-efficiency mcrodisk lasers such as thresholdless laser and single photon source.